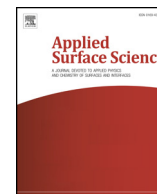




Contents lists available at ScienceDirect

Applied Surface Science

journal homepage: [www.elsevier.com/locate/apsusc](http://www.elsevier.com/locate/apsusc)

Full length article

# Magnetoelectric composite films of $\text{La}_{0.67}\text{Sr}_{0.33}\text{MnO}_3$ and Fe-substituted $\text{Bi}_4\text{Ti}_3\text{O}_{12}$ fabricated by chemical solution deposition

Zongfan Duan<sup>a,b,\*</sup>, Xing Fu<sup>a</sup>, Zhu Yang<sup>a</sup>, Yun Mei<sup>a</sup>, Jie Cui<sup>a,b,\*</sup>, Jiqiang Jia<sup>a</sup>, Li Ma<sup>a</sup>, Caiyin You<sup>a</sup>, Gaoyang Zhao<sup>a,b</sup>

<sup>a</sup> School of Materials Science and Engineering, Xi'an University of Technology, Xi'an 710048, China

<sup>b</sup> Shaanxi Key Laboratory of Electrical Materials and Infiltration Technology, Xi'an 710048, China



## ARTICLE INFO

## Keywords:

Multiferroic  
Magnetoelectric coupling effect  
 $\text{Bi}_4\text{Ti}_3\text{O}_{12}$   
Fe substitution  
Silicon substrate

## ABSTRACT

Magnetoelectric composite layered films of  $\text{La}_{0.67}\text{Sr}_{0.33}\text{MnO}_3$  (LSMO) and Fe-substituted  $\text{Bi}_4\text{Ti}_3\text{O}_{12}$  ( $\text{Bi}_4\text{Ti}_{3-x}\text{Fe}_x\text{O}_{12}$ ,  $\text{BiTF}_x$ ,  $x = 0.05, 0.10, 0.15$  and  $0.20$ ) were fabricated on a  $\text{LaNiO}_3$ -buffered silicon substrate by chemical solution deposition method. The  $\text{LaNiO}_3$  layer with  $c$ -axis orientation can not only induce the oriented growth of the overlying LSMO and  $\text{BiTF}_x$  layers, but also can act as an electrode material for electric measurements. The Fe-substituted content has a significant effect on the surface morphology of  $\text{BiTF}_x$  phase, and leakage, dielectric and ferroelectric properties of the  $\text{BiTF}_x/\text{LSMO}$  films. The  $\text{BiTF}_{0.10}/\text{LSMO}$  composite film exhibits an improved leakage performance, the highest dielectric constant and the best ferroelectric properties. Furthermore, an interesting finding is that a weak ferromagnetism is present in the  $\text{BiTF}_{0.10}$  phase. The first-principle calculations suggest that the spin-resolved total density of states for  $\text{BiTF}_{0.10}$  are asymmetric, which can induce spin splitting and magnetic moments. The  $\text{BiTF}_{0.10}/\text{LSMO}$  film also exhibits excellent magnetoelectric coupling performance, and its magnetoelectric coupling response is sensitive to AC magnetic frequency. The highest magnetoelectric coupling voltage coefficient can reach up to  $47.5 \text{ V/cm}\cdot\text{Oe}$  without the presence of DC bias magnetic field.

## 1. Introduction

Multiferroic materials with ferroelectric and magnetic orders present ferroelectric and magnetic and/or ferroelastic properties. The most attractive characteristic of these materials is the magnetoelectric coupling (ME) effect, which refers to an induced electron polarization under an external magnetic field or an induced magnetization with the presence of an applied electric field. Since the ME effect provides a promising route to develop new devices, it gives rise to an increasing interest in multiferroic field [1–10]. Unfortunately, a very weak ME effect was observed in the single-phase multiferroic materials at room temperature, hindering its wide applications. To tackle this issue, a number of researchers are engaged in the development of new magnetoelectric composites.

In the past decades, many magnetoelectric composite films have been prepared by different combinations of ferroelectric [e.g.,  $\text{PbTiO}_3$ ,  $(\text{Pb,Zr})\text{TiO}_3$ ,  $\text{BiFeO}_3$  and  $\text{BaTiO}_3$ ] and ferromagnetic [e.g.,  $\text{CoFe}_2\text{O}_4$  and  $(\text{La,Sr})\text{MnO}_3$ ] materials. However, the magnetoelectric composite films with high ME voltage coefficient ( $\alpha_p$ ) reaching  $\text{V/cm}\cdot\text{Oe}$  magnitude, is still seldom reported [11–14].  $\text{Bi}_4\text{Ti}_3\text{O}_{12}$  (BiT) and substituted-BiT are

bismuth layer structure perovskites, and exhibit excellent polarization and piezoelectric properties. More attractively, these materials without lead element are environmentally friendly. Hence, BiT and substituted-BiT could be potential environment-friendly ferroelectric components of magnetoelectric composite films [15]. However, this has rarely been investigated so far. At present, substitution modification of BiT is a hot topic in the field of multiferroic materials. It has been proved that the ferroelectric properties of BiT can be enhanced by an appropriate ion substitution at its Bi-site (A-site) or/and Ti-site (B-site) [16,17]. On the other hand, a few studies focused on the magnetic ion substitution of ferroelectric materials, and the ferromagnetism have been successfully introduced into  $\text{BaTiO}_3$  and  $\text{PbTiO}_3$  [18–22]. Kimura et al. believed that magnetic ion substituted Aurivillius compounds with multiferroic properties are derived from the change of magnetic ordering [23]. Nevertheless, few literatures have been reported on the substitution modification of BiT by magnetic ion (such as Fe, Mn and Co ions) [24–30]. Bark et al. prepared a series of Fe-La co-substituted BiT powders and demonstrated that a small amount of Fe substitution can not only modify the electronic structure of BiT based oxides, but also tune their band-gaps [27]. Shashkovet et al. reported that high

\* Corresponding authors at: School of Materials Science and Engineering, Xi'an University of Technology, Xi'an 710048, China.

E-mail addresses: [duanzf@xaut.edu.cn](mailto:duanzf@xaut.edu.cn) (Z. Duan), [Cuijie@xaut.edu.cn](mailto:Cuijie@xaut.edu.cn) (J. Cui).

<https://doi.org/10.1016/j.apsusc.2019.06.030>

Received 27 February 2019; Received in revised form 25 May 2019; Accepted 3 June 2019

Available online 07 June 2019

0169-4332/© 2019 Elsevier B.V. All rights reserved.

concentration of Fe substitution could increase the number of perovskite-like layers separated by bismuth layers ( $\text{Bi}_2\text{O}_3$ )<sup>2+</sup>, resulting in substantial changes in microstructure and dielectric properties of Fe-substituted BiT ceramics [28]. Chen et al. have suggested that partly substitution Ti with Fe in BiT ceramics cannot change the layered perovskite structure of BiT, but can enhance its remnant polarization [29]. Xia et al. reported that Fe substitution can change the surface morphology and electric properties of BiT film. However, the optimum substitution amount of Fe ion in BiT is still unknown, and its ferromagnetism and mechanism of magnetic generation have also not been investigated [30]. Moreover, no research work has been conducted on the preparation of magnetoelectric composite films utilizing Fe-substituted BiT as a ferroelectric phase.

Due to the features of lower cost, larger area and volume production, silicon substrates have been widely used in semiconductor field. Recently, there is a trend towards incorporating many functions into silicon substrates. Since the crystal orientation of the magnetoelectric composite film has a significant effect on the ferromagnetism, ferroelectricity and ME performance, it is necessary to regulate the oriented growth of the magnetoelectric composite film on silicon substrate. However, large lattice mismatch between the ferromagnetic/ferroelectric phase and the silicon substrate causes some additional strain and random growth of the overlying ferroelectric/ferromagnetic phase. Fortunately, the oriented  $\text{LaNiO}_3$  (LNO) film coated on silicon substrate can act as a seed layer to induce the oriented growth of the overlying perovskite ferromagnetic (or ferroelectric) layer. Moreover, it has been proved that LNO not only can be used as an electrode material to replace precious metals, but also improve fatigue performance of ferroelectric films [31–34]. Subsequently, it is desirable to utilize an oriented LNO film as the buffer layer and/or bottom electrode to integrate magnetoelectric composite films on the silicon substrate.

In this work,  $\text{La}_{0.67}\text{Sr}_{0.33}\text{MnO}_3$  (LSMO) with large magnetostriction and high saturation magnetization was used as a ferromagnetic phase [35], Fe-substituted BiT ( $\text{Bi}_{4-x}\text{Fe}_x\text{O}_{12}$ ,  $\text{BiTF}_x$ ,  $x = 0.05, 0.10, 0.15$  and  $0.20$ ) was used as a ferroelectric phase, and they were sequentially deposited onto *c*-axis oriented LNO-buffered silicon substrates. As a result, several 2-2 type magnetoelectric composite ( $\text{BiTF}_x/\text{LSMO}$ ) films were prepared. Considering the advantages of chemical solution deposition (CSD) method, such as facile control of chemical composition and low cost, all layers were fabricated by CSD. The effect of Fe-substituted content on the surface morphology of  $\text{BiTF}_x$  phase, and leakage, dielectric and ferroelectric properties of the  $\text{BiTF}_x/\text{LSMO}$  films was studied, and the optimum Fe-substituted content was determined. The ferromagnetism of the  $\text{BiTF}_{0.10}$  film with optimum Fe-substituted content was examined and the mechanism of magnetic generation was discussed. Finally, ME properties of the  $\text{BiTF}_{0.10}/\text{LSMO}$  film were well investigated.

## 2. Experimental

The silicon substrate with (001) orientation was commercially obtained from Hefei Ke Jing Materials Technology Co., Ltd. Other reagents with analytic grade were purchased from Sinopharm Chemical Reagent Co., Ltd. and used as received. The precursor solutions and dip-coating for gel films were prepared at room temperature in the glove box with a relative humidity of 30%.

The details of the preparation process for LNO film can be referenced in our recent publication [36]. The heating rate of  $40^\circ\text{C/s}$  was used during the rapid heat treatment process and the obtained LNO film had an average resistivity of  $9.4 \times 10^{-4} \Omega\text{cm}$ . The LSMO/LNO film was prepared by subsequent deposition of LSMO layer onto the as-prepared LNO layer. The preparation procedure of LSMO layer was the same as that described in our previous study [37]. To deposit  $\text{BiTF}_x$  layers,  $\text{BiTF}_x$  precursor solutions were prepared beforehand. The volume of the prepared  $\text{BiTF}_x$  solutions and the total metal ion concentration were 15 mL and 0.7 mol/L, respectively. The required

**Table 1**

The required amounts of main reagents for  $\text{BiTF}_x$  precursor solutions.

$\text{BiTF}_x$	$\text{Bi}(\text{NO}_3)_3 \cdot 5\text{H}_2\text{O}/$ (g)	$\text{Fe}(\text{NO}_3)_3 \cdot 9\text{H}_2\text{O}/$ (g)	$\text{Ti}(\text{OC}_4\text{H}_9)_4/$ (g)	Acetyl acetone/(g)
$\text{BiTF}_{0.05}$	3.201	0.030	1.506	1.482
$\text{BiTF}_{0.10}$	3.201	0.061	1.481	1.457
$\text{BiTF}_{0.15}$	3.201	0.091	1.455	1.432
$\text{BiTF}_{0.20}$	3.201	0.121	1.425	1.402

amounts of main reagents were listed in Table 1.

The detail preparation process is as follows:  $\text{Bi}(\text{NO}_3)_3 \cdot 5\text{H}_2\text{O}$  and  $\text{Fe}(\text{NO}_3)_3 \cdot 9\text{H}_2\text{O}$  were alternately added in turn to the 5 mL 2-methoxyethanol, followed by magnetical stirring for 3 h to get a transparent dark-brown solution. Meanwhile, acetyl acetone and  $\text{Ti}(\text{OC}_4\text{H}_9)_4$  were successively dissolved into another 5 mL 2-methoxyethanol to obtain a light-yellow solution. After that, two solutions were mixed, and then an appropriate amount of 2-methoxyethanol was supplemented to adjust the volume of the mixed solution to 15 mL. Finally, several stable and uniform  $\text{BiTF}_x$  solutions were obtained after magnetical stirring for 8 h followed by aging for 12 h. The  $\text{BiTF}_x$  gel layers were fabricated on LSMO/LNO films using a dip coater with a drawing rate of 0.5 mm/s. They were firstly dried at  $200^\circ\text{C}$  for 10 min to volatilize solvent and decompose partial organics, then heated up to  $730^\circ\text{C}$  at a rapid thermal annealing furnace with a heating rate of  $40^\circ\text{C/s}$ . Finally, the samples were completely crystallized at  $730^\circ\text{C}$  for 10 min. To obtain the desired thickness of  $\text{BiTF}_x$  layers, above procedures were repeated 8 times.

Crystal structure was characterized by a grazing incidence X-ray diffraction (GI-XRD, XRD-7000, Shimadzu) with  $\text{CuK}\alpha$  radiation. Raman spectra of  $\text{BiTF}_x$  powders were performed on a Laser Raman spectrometer (Renishaw inVia plus). An X-ray photoelectron spectroscopy (XPS, ESCALAB-250Xi) with  $\text{AlK}\alpha$  line was used to examine the chemical compositions and ion valences of samples, and all binding energy values were calibrated by the C 1s peak at 284.8 eV of the surface adventitious carbon. The morphology was analysed by a field emission scanning electron microscopy (FE-SEM, Zeiss MERLIN). The leakage behaviors and ferroelectric properties of the composite films were detected by a ferroelectric testing apparatus (TF-Analyzer, 2000, aixACCT). An impedance analyzer (Agilent 4284A) was applied to examine the dielectric behaviors of the films. Magnetic measurement was performed using a vibrating sample magnetometer (VSM, Lake Shore 7400) with an error of 0.5%. The magnetometer was calibrated using a standard sample (Nickel ball) in advance and the direction of the magnetic field was perpendicular to the film plane. A ME measuring device (Super-ME, Quantum Design China) was used to characterize ME performance of the  $\text{BiTF}_{0.10}/\text{LSMO}$  film. It consists of an electromagnet and a Helmholtz coil, which can provide a direct-current (DC) bias magnetic field ( $H_{\text{bias}}$ ) and an alternating-current (AC) magnetic field, respectively. The sample was placed in the middle of the Helmholtz coil, and the  $H_{\text{bias}}$  was imposed perpendicular to the plane of the film. A lock-in amplifier was applied to monitor ME output voltages. All measurements were carried out at room temperature.

The density of state and electronic structure of  $\text{BiTF}_{0.10}$  was investigated by first-principles calculations based on density functional theory (DFT) as implemented in the Vienna ab initio simulation package (VASP) code [38]. The exchange and correlation energy was described by the generalized gradient approximation of Perdew, Burke, and Ernzerhof (PBE) [39,40]. The projected augmented wave (PAW) method was employed with the energy cutoff of 450 eV. The Brillouin zone was sampled by  $5 \times 5 \times 1$  and  $9 \times 9 \times 1$  meshes during the optimization and DOS calculations, respectively [41].

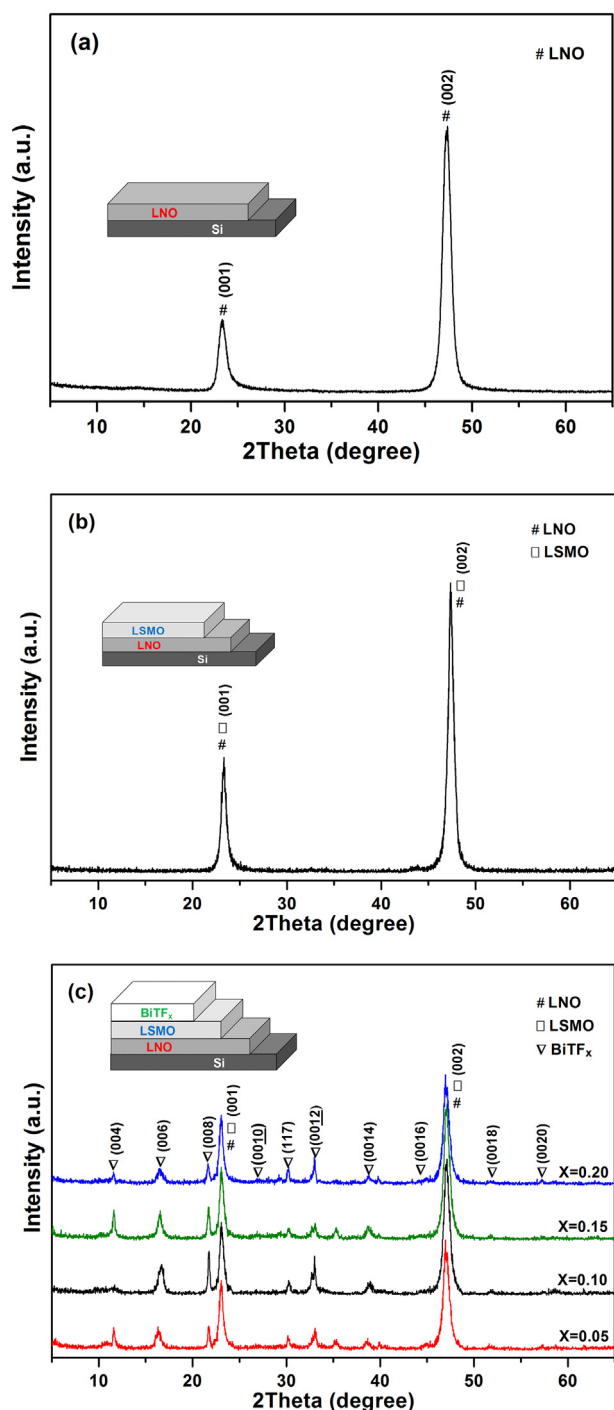


Fig. 1. GI-XRD patterns of LNO (a), LSMO/LNO (b) and BiTF<sub>x</sub>/LSMO/LNO (c) films.

### 3. Result and discussion

#### 3.1. GI-XRD analysis

Fig. 1(a)–(c) are the GI-XRD patterns of LNO, LSMO/LNO and BiTF<sub>x</sub>/LSMO/LNO films, respectively. As shown in Fig. 1(a), the dominant peaks of the LNO film are (001) and (002), suggesting the high degree of *c*-axis preferential orientation. For the LSMO/LNO film, both (001) and (002) peaks of the LSMO layer are completely emerged in those of the LNO layer, see Fig. 1(b). As determined by the JCPDS standards, the lattice parameter of the pseudocubic LSMO is 0.387 nm (card No. 33-0710), which is quite close to that of the LNO (0.384 nm,

Card No.50–0308). The calculated lattice mismatch between them is only 2.1%, resulting in the *c*-axis oriented growth of the LSMO layer on the LNO seed layer. As for the BiTF<sub>x</sub>/LSMO/LNO films with various Fe-substituted contents (Fig. 1(c)), except that strong (001) and (002) peaks belong to LSMO/LNO layer, the other peaks are completely indexed on the base of a pseudo-orthorhombic cell for a single BiT (Card No. 35-0795), and no any extra reflections corresponding to impurity phases are observed. Although four kinds of composite films have different Fe-substituted contents, there is no any significant difference in their XRD patterns. This suggests that the Fe ions dissolve in the BiT, and Fe-substitution does not change the bismuth-layered perovskite structure of BiT. Similar results were also reported by Yamamoto et al. in the study of substitution mechanism of Fe in the sole phase BiT polycrystalline using X-ray absorption near-edge structure measurements and first-principles calculations [42]. No additional phases except for LNO, LSMO and BiTF<sub>x</sub> are observed, which implies that no diffusion reaction occurs among these phases. Besides the weak (117) diffraction peak, the dominated (00*l*) (*l* = 4, 6, 8, and etc.) peaks can be observed for the BiTF<sub>x</sub> layer. This indicates that the BiTF<sub>x</sub> layers also present an excellent *c*-axis orientation. The proportion of the *c*-axis orientated grains,  $\alpha(00l)$ , was estimated using Lotgering method, which can be expressed as Eq. (1) [43].

$$\alpha(00l) = \frac{\sum \frac{I_{(00l)}}{I_{(00l)}^*}}{\sum \frac{I_{(hkl)}}{I_{(hkl)}^*}} \quad (1)$$

where  $I_{(00l)}$  and  $I_{(hkl)}$  are the measured intensities of (00*l*) and (*hkl*) diffraction peaks of the prepared film samples, and  $I_{(00l)}^*$  and  $I_{(hkl)}^*$  are intensities of (00*l*) and (*hkl*) diffraction peaks referring the standard PDF card of BiT, respectively. The estimated  $\alpha(00l)$  values of BiTF<sub>x</sub> (*x* = 0.05, 0.10, 0.15, 0.20) layers are 90.5%, 97.8%, 97.1% and 56.8%, respectively. Obviously, the Fe-substituted content has a significant effect on the *c*-axis orientation degree of the BiTF<sub>x</sub> layer, and the BiTF<sub>0.10</sub>/LSMO film exhibits the highest *c*-axis orientation degree. For the BiTF<sub>0.20</sub>/LSMO film, the degree of orientation decreases significantly. It is likely that Fe-rich precipitates formed at grain boundaries affect the orientation growth of grains. This will be further discussed in the subsequent SEM analysis.

#### 3.2. Raman characterization

Raman spectra are very sensitive to the interfacial stress. To exclude the impact of the stress derived from the underlayer and the substrate, BiTF<sub>x</sub> powders were used for Raman spectra measurement. The BiTF<sub>x</sub> powders were prepared from BiTF<sub>x</sub> solutions by drying at 80 °C for 24 h, followed by annealing at 730 °C for 1 h in an electric furnace. Fig. 2(a) and (b) are the Raman spectra of BiTF<sub>x</sub> powders and the variation of the wavenumber around 540 cm<sup>−1</sup> with Fe-substituted content, respectively. As shown in Fig. 2(a), the low frequency modes (< 200 cm<sup>−1</sup>) can be attributed to the motion of Bi<sup>3+</sup> ions, whereas the higher frequency modes (> 200 cm<sup>−1</sup>) are classified as the TiO<sub>6</sub> octahedra structure of the BiTF<sub>x</sub> [44,45]. The modes at 119–120 cm<sup>−1</sup> assigning as the Bi<sup>3+</sup> vibration, have no change with increase of Fe-substituted content, showing that Fe substitution has little effect on the A-site Bi<sup>3+</sup>. However, for the higher frequency modes, new weak modes can be observed at 686 cm<sup>−1</sup> in the BiTF<sub>0.15</sub> and BiTF<sub>0.20</sub> samples. These modes can be classified as the Bi-O-Fe vibrations of the perovskite block, which can confirm that Fe atoms enter into the lattice of BiT. Furthermore, the modes of Ti<sup>4+</sup> vibration around 227, 265, 324, 540, 568 and 850 cm<sup>−1</sup> gradually widened with the increase of Fe-substituted content. This indicates that the Fe substitution has an impact on the vibration modes of the TiO<sub>6</sub> octahedra, giving rise to the considerable distortion of TiO<sub>6</sub> octahedra. Liu et al. reported that the mode corresponding to the opposite excursion of the external apical O atoms of the TiO<sub>6</sub> octahedra in the BiT powder located at 537 cm<sup>−1</sup> [45].

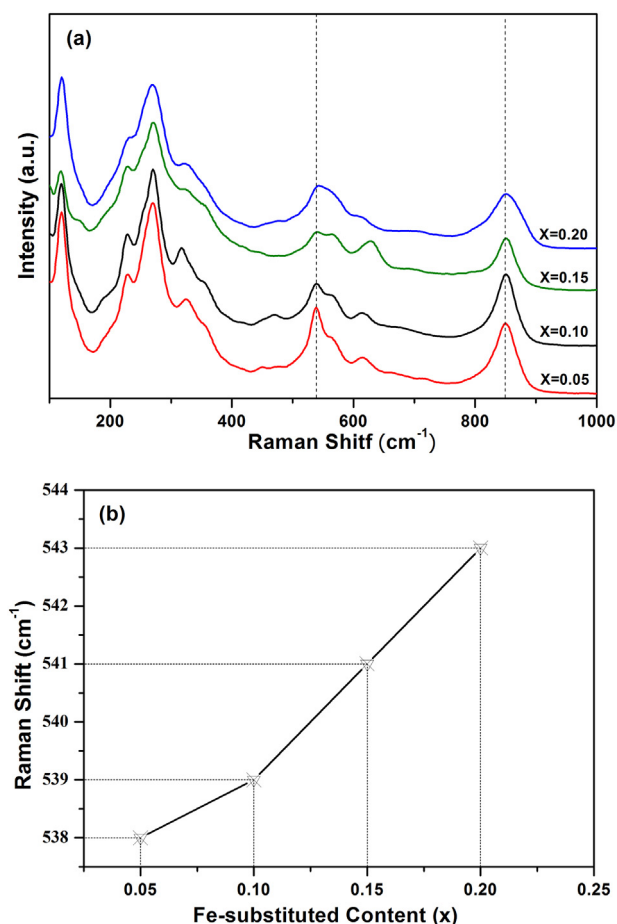


Fig. 2. Raman spectra of BiTF<sub>x</sub> powders (a) and the variation of the wavenumber around 540 cm<sup>-1</sup> with Fe-substituted content (b).

Nevertheless, as shown in Fig. 2(b), the corresponding vibrational wavenumbers in the BiTF<sub>x</sub> samples are larger than that of BiT powder (537 cm<sup>-1</sup>), and the wavenumber shifts from 538 to 543 cm<sup>-1</sup> as the Fe-substituted content (x) increases from 0.05 to 0.20. This is because that the valence of Fe ion in BiTF<sub>x</sub> is mainly +3, and the ionic radius of Fe<sup>3+</sup> (0.0550 nm) is less than that of Ti<sup>4+</sup> (0.0559 nm) [46,47]. The Fe<sup>3+</sup> substitution for Ti<sup>4+</sup> inevitably causes the octahedral distortion in BiTF<sub>x</sub>, resulting in the upshifting of the Raman spectra.

### 3.3. XPS characterization

To elucidate the chemical compositions of the BiTF<sub>x</sub> films and valences of Bi, Ti, O and Fe ions, surface analysis was performed on the BiTF<sub>0.10</sub> film by XPS. As presented in Fig. 3(a), all observed peaks are corresponding to Bi, Ti, O and adventitious carbon. Therefore, except for the adventitious carbon, no impurity element was detected. The narrow scan spectrum of Bi is shown in Fig. 3(b). It can be found from Fig. 3(b) that Bi 4f exhibits a doublet peaks with the bond energies of 158.6 and 164.0 eV, which correspond to Bi 4f<sub>7/2</sub> and Bi 4f<sub>5/2</sub> levels of Bi<sup>3+</sup>, respectively [48]. The Ti 2p spin-orbit has a doublet peaks (Fig. 3(c)), located at 457.4 and 465.8 eV, which are attributed to Ti 2p<sub>3/2</sub> and Ti 2p<sub>1/2</sub> levels of Ti<sup>4+</sup>, respectively [49]. As shown in Fig. 3(d), the Fe 2p spin-orbit also exhibits a doublet peaks. The low peak (724.7 eV) and the high peak (711.6 eV) are ascribed to Fe 2p<sub>1/2</sub> and Fe 2p<sub>3/2</sub> levels of Fe<sup>3+</sup>, respectively. This result indicates that, although Fe generally has +2 and +3 valence states, the Fe ion in BiTF<sub>x</sub> exists mainly in the form of Fe<sup>3+</sup> [50]. The spectrum of O1s, can be fitted by two peaks, see Fig. 3(e). The major one (529.6 eV) is attributed to the lattice O in BiTF<sub>0.10</sub> matrix, while the minor one

(531.4 eV) is ascribed to the oxygen vacancy [51].

### 3.4. Microstructure analysis

As shown in Fig. 4(a), the LNO film exhibits a polycrystalline microstructure, whereas no pinholes and cracks can be observed. The LNO film is comprised of irregular granular grains with an average size of 100 nm. Its good surface quality is beneficial for the oriented growth of the overlying ferromagnetic LSMO layer on it. As seen from Fig. 4(b), there are many fine pinholes though the LSMO layer. Even so, the surface quality of the as-prepared LSMO layer is superior to the LSMO film prepared by the same CSD method reported in the literature [52]. The morphologies of the BiTF<sub>x</sub> layers are shown in Fig. 4(c)–(f). As shown in Fig. 4(c), no cracks and pinholes can be observed in BiTF<sub>0.05</sub> layer, which is consisted of homologous plate-like grains with an average size above 300 nm. The plane of the most plate-like grains is parallel to the substrate surface. Similar surface morphology is observed in many BiT films with high c-axis orientation degree [53,54]. The BiTF<sub>0.10</sub> layer also exhibits plate-like grain, while its grain size (about 250 nm) is obviously less than that of the BiTF<sub>0.05</sub> layer. This may be ascribed to the lattice distortion induced by Fe substitution. Generally, the high substituted concentration leads to a serious lattice distortion, which may reduce the growth rate of grains. Though the surface morphology, has no obvious difference between BiTF<sub>0.15</sub> layer and BiTF<sub>0.10</sub> layer, the BiTF<sub>0.20</sub> layer with the largest Fe-substituted content presents a different surface profile. As shown in Fig. 4(f), the BiTF<sub>0.20</sub> layer is mainly composed of granular grains with an average grain size of 200 nm. However, some spherical precipitates with a diameter of about 30 nm can be observed at the grain boundaries of large grains at higher magnification, see Fig. 4(g). Fig. 4(h) is the energy dispersive X-ray spectrometry (EDS) analysed results of the spherical precipitate. It is learnt from Fig. 4(h) that the Fe content (1.88 wt%) is larger than the stoichiometric concentration of Bi<sub>4</sub>Ti<sub>2.8</sub>Fe<sub>0.20</sub>O<sub>12</sub> (0.95wt.%Fe). This indicates that Fe-substituted content x = 0.20 exceeds the maximum solid solubility in BiT at x = 0.20. Due to the limited detection of the XRD instrument, the precipitates were not detected by GI-XRD (see Fig. 1(c)). As a result, the formation of precipitates with high concentration of Fe<sup>3+</sup> at the grain boundaries may influence the nucleation and growth of grains, causing the change of grain morphology from plate-like to granular shape. As determined by Fig. 4(i), the thicknesses of the BiTF<sub>0.10</sub>, LSMO and LNO layer are approximately 226, 128 and 245 nm, respectively.

### 3.5. Leakage properties

As for the conductive metal oxide, the as-prepared LNO layer has excellent conductivity. It was directly used as the bottom electrode for electronic measurements. Fig. 5 illustrates the leakage characteristics of the BiTF<sub>x</sub>/LSMO films as the function of direct current electric field (E). At an electric field of 200 kV/cm, the leakage current density (J) of the BiTF<sub>0.05</sub>/LSMO film is  $1.2 \times 10^{-5}$  A/cm<sup>2</sup>, which is decreased by more than one order of magnitude in comparison with that of BiT/LSMO film ( $4.3 \times 10^{-4}$  A/cm<sup>2</sup>) at the same electric field [17]. Obviously, the improvement of leakage performance is ascribed to Fe substitution. The J values for BiTF<sub>x</sub>/LSMO (x = 0.05, 0.10, 0.15 and 0.20) films at the maximum electric field of 500 kV/cm are  $4.9 \times 10^{-5}$ ,  $3.3 \times 10^{-6}$ ,  $6.8 \times 10^{-6}$  and  $2.5 \times 10^{-5}$  A/cm<sup>2</sup>, respectively. This demonstrates that J of the BiTF<sub>x</sub>/LSMO film decreases and then increases with the increase of the Fe-substituted content, and the optimum Fe-substituted content for BiTF<sub>x</sub> phase is x = 0.10. To figure out the conduction mechanism of the BiTF<sub>x</sub>/LSMO films, the curves of ln(J) versus ln(E) were plotted, as shown in Fig. 5(b). The curves show two linear segments for the BiTF<sub>x</sub>/LSMO (x = 0.05 and 0.20) films. The slope values (S) of the front part are 1.36 and 1.30, respectively, which is approximate 1. It suggests an Ohmic conduction mechanism. For Ohmic conduction mechanism, electric current mainly derives from the thermally excited



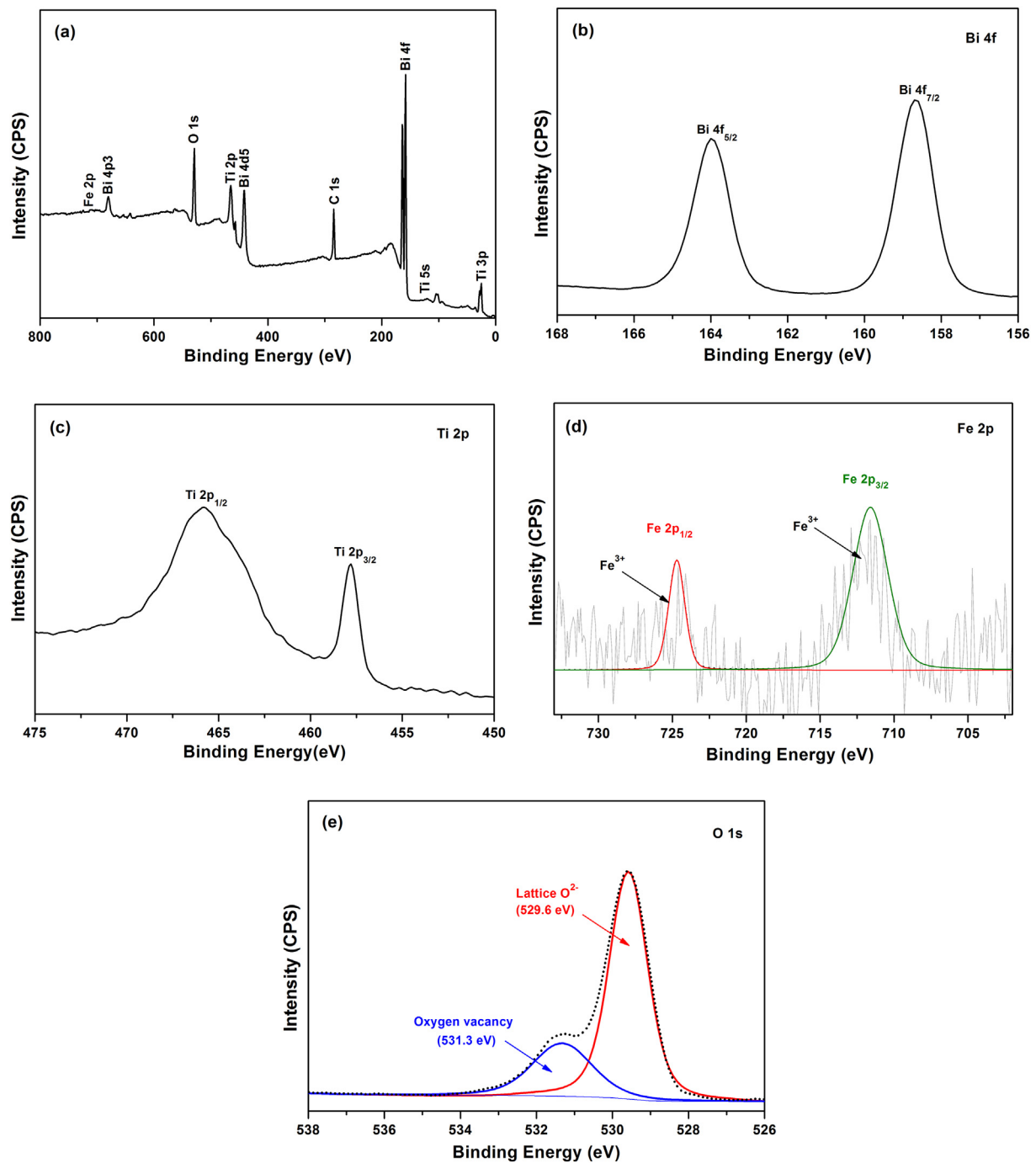


Fig. 3. XPS spectra of BiTF<sub>0.10</sub> film: (a) wide-scan spectrum and narrow scan spectra of (b) Bi 4f, (c) Ti 2p, (d) Fe 2p and (e) O 1s.

electrons [55,56]. Nevertheless,  $S$  values of the latter half with higher electrical field are 1.63 and 1.89, respectively, which are approximately equal to 2. The value of  $S$  is changed in the range of 1 to 2, suggesting that a space charge limited conduction (SCLC) mechanism emerges [57,58]. In SCLC mechanism, due to the carrier injection, the concentration of free electrons is larger than that of thermally excited electrons. The injected free electrons from electrodes to the film will increase with the increase of the applied electrical field. For strong electron injection, a trap-filled limited conduction mechanism is dominated, the traps in the film will be filled up and a large amount of space charge will be generated. Therefore, the leakage current of the films will inevitably increase under high electric fields. As for the BiTF<sub>0.20</sub>/LSMO film, the impurity phase segregated at the boundaries

may act as the defect to result in the occurrence of space charges, which may lead to the significant deterioration of leakage performance. However, the BiTF<sub>x</sub>/LSMO ( $x = 0.10$  and  $0.15$ ) films display a linear curve with slope ( $S$ ) values of 1.18 and 1.24, respectively, which are approximate to 1. It suggests that these films exhibit a unique Ohmic conduction mechanism. Generally, the Ohmic conduction mode occurred in the insulating film, is favourable for good leakage performance. Compared with that of BiTF<sub>0.15</sub>/LSMO film, the  $S$  value of the BiTF<sub>0.10</sub>/LSMO film is closer to 1, indicating that there are fewer defects in the BiTF<sub>0.10</sub>/LSMO film. Owing to outstanding leakage performance, good ferroelectric and dielectric properties of the BiTF<sub>0.10</sub>/LSMO will be expected. In the previous study, it has been widely recognized that the substitution in B-site of BiT by the ions with large radius or higher

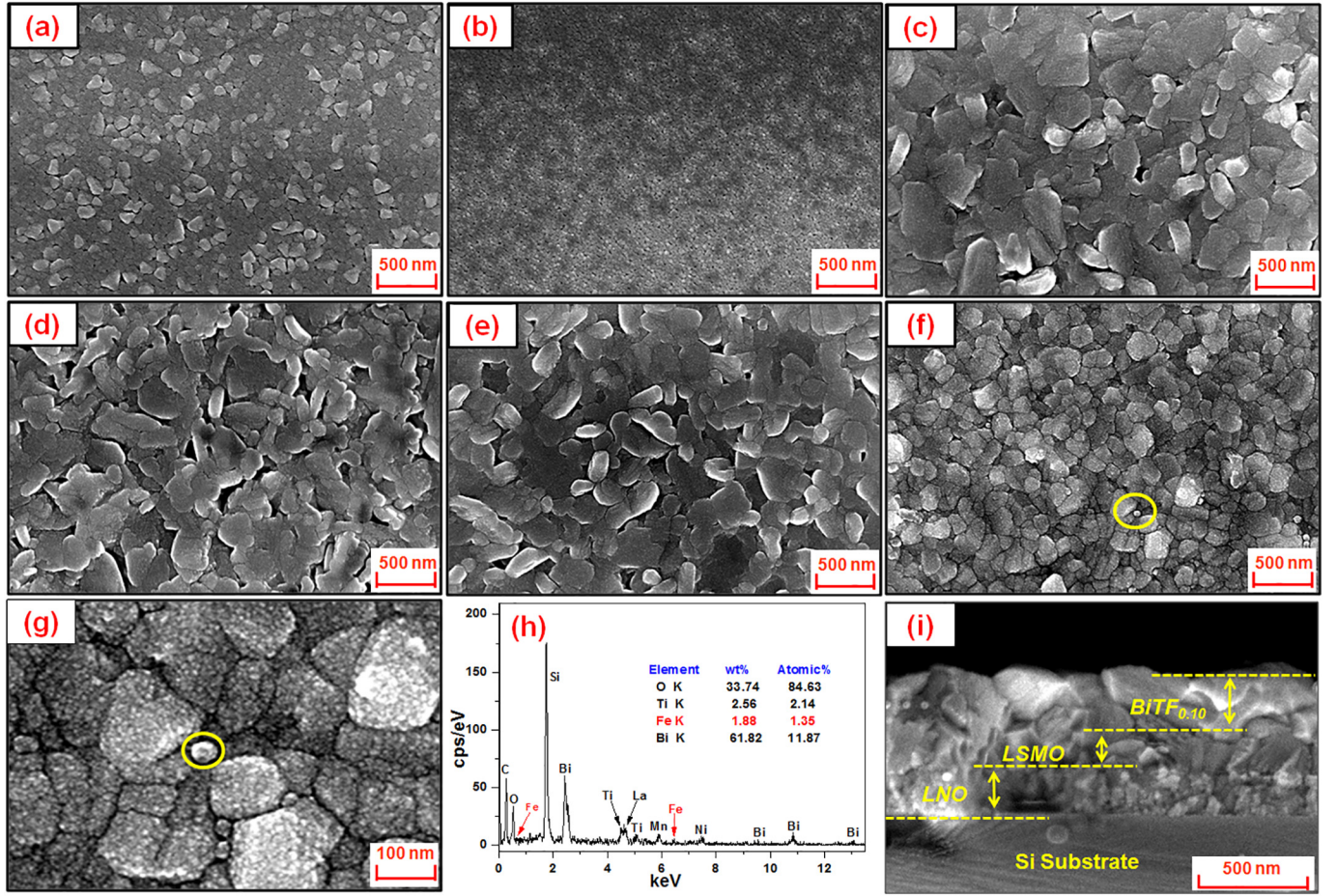


Fig. 4. SEM images of LNO (a), LSMO (b), BiTF<sub>0.05</sub> (c), BiTF<sub>0.10</sub> (d), BiTF<sub>0.15</sub> (e) and BiTF<sub>0.20</sub> (f) layers, (g) selected area EDS of BiTF<sub>0.20</sub> layer and (h) cross-sectional micrograph for BiTF<sub>0.10</sub>/LSMO/LNO/Si.

charge valences is more effective to improve its leakage performance [59,60]. However, compared with those of the Ti<sup>4+</sup>, Fe<sup>3+</sup> as substitute ion has a smaller ionic radius and lower valence. The BiTF<sub>x</sub> is likely to have different leakage improvement mechanism. It can be attributed to the defect reaction as follow:



Because the oxygen vacancy ( $V_{O}^{\bullet}$ ) is trapped by  $Fe_{Ti}'$  defect, leading to that oxygen vacancy cannot trap electrons, it is inevitable that the BiTF<sub>x</sub> films have an improved leakage performance.

### 3.6. Dielectric behaviors

The variations of the dielectric constant ( $\epsilon_r$ ) and the dissipation factor ( $\tan\delta$ ) with electric frequency of the BiTF<sub>x</sub>/LSMO films are shown in Fig. 6. The  $\epsilon_r$  values of films are ranged from 187 to 228 at the frequency of 100 Hz, which are comparable to those of Nd-Zr co-substituted BiT film prepared by CSD method [61] and Sm substituted BiT film prepared by pulsed laser deposition (PLD) method [62]. Furthermore, the  $\epsilon_r$  of the prepared films decreases with electric frequency. This is likely attributed to the extrinsic resonance behavior induced by the microstructure defect of the film [63]. For all prepared films, the  $\tan\delta$  values do not exceed 0.11 in the range of 0.1–100 kHz. As a fore mentioned, it is thought that the BiTF<sub>0.10</sub>/LSMO film possesses the largest  $\epsilon_r$  and the smallest  $\tan\delta$ , which may be attributed to its excellent leakage characteristic.

### 3.7. Ferroelectric performance

The polarization-electric field ( $P$ - $E$ ) hysteresis loops of the BiTF<sub>x</sub>/LSMO films are presented in Fig. 7(a). Among these films, the BiTF<sub>0.10</sub>/LSMO film exhibits a relatively well saturated  $P$ - $E$  curve, which is due to its good leakage performance. The variations of the residual polarization ( $P_r$ ) and coercive field ( $E_c$ ) values with Fe-substituted contents are depicted in Fig. 7(b). It can be seen that the  $P_r$  increases and then decreases with increase of Fe-substituted content, while the  $E_c$  presents an opposite change. At  $x = 0.10$ , the BiTF<sub>x</sub>/LSMO film possesses the highest  $P_r$  of 28.7  $\mu\text{C}/\text{cm}^2$ , and the lowest  $E_c$  of 213 kV/cm, suggesting the best ferroelectric properties. This  $P_r$  value is comparable to that of Bi<sub>4</sub>Ti<sub>2.94</sub>Fe<sub>0.03</sub>O<sub>12</sub> ferroelectric film deposited on SnO<sub>2</sub>:F/glass substrate prepared by CSD method [30], which is also higher than that of some substituted-BiT films prepared by PLD method, such as Nd-substituted BiT film with Pt/Ti/SiO<sub>2</sub> substrate [64] and Hf-substituted BiT film with SrTiO<sub>3</sub> single-crystal substrate and SrRuO<sub>3</sub> bottom electrode [65]. As mentioned above, the ionic radius of Fe<sup>3+</sup> is smaller than that of Ti<sup>4+</sup> in BiT. As host Ti<sup>4+</sup> is substituted by small Fe<sup>3+</sup>, which will be located at the off-centered position, and thus, leads to the distortion of TiO<sub>6</sub> octahedra. As a consequence, ferroelectric polarization will be enhanced [66]. For the ferroelectrics,  $E_c$  is thought to be closely related to the pinning effect of space charge. The sole Ohmic conduction mode of the BiTF<sub>0.10</sub>/LSMO film suggests its good leakage performance and weak space charge effect. Consequently, the BiTF<sub>0.10</sub>/LSMO film exhibits the lowest  $E_c$ . As discussed above, when the Fe-substituted content  $x$  is above 0.15, the  $P_r$  value of the films begins to drop, while the  $E_c$  values rise up. Especially, the BiTF<sub>0.20</sub>/LSMO film exhibits the lower  $P_r$  and higher  $E_c$ . This can be attributed to the occurrence of impurity

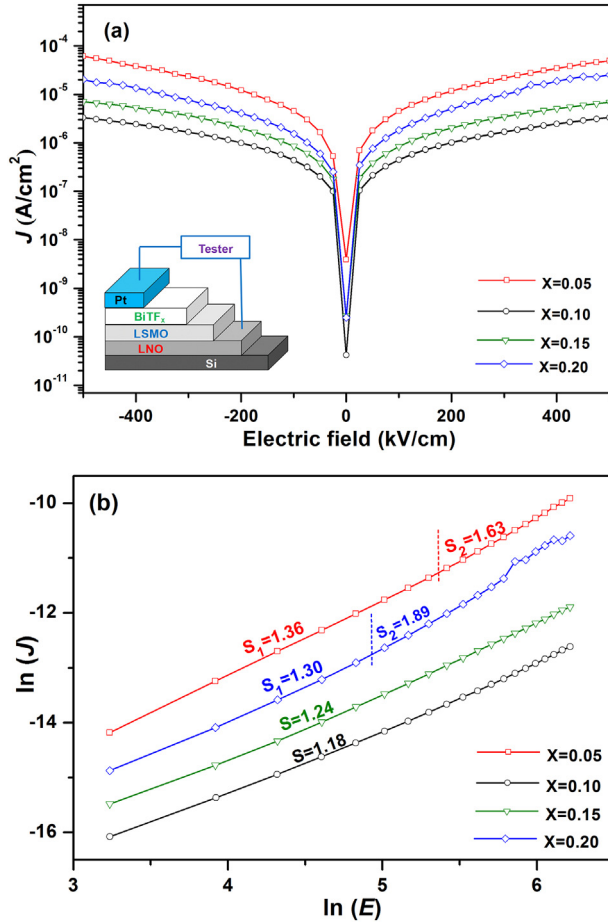


Fig. 5. Leakage properties of BiTF<sub>x</sub>/LSMO films: (a)  $J$  vs.  $E$  curve and (b)  $\ln(J)$  vs.  $\ln(E)$  curve.

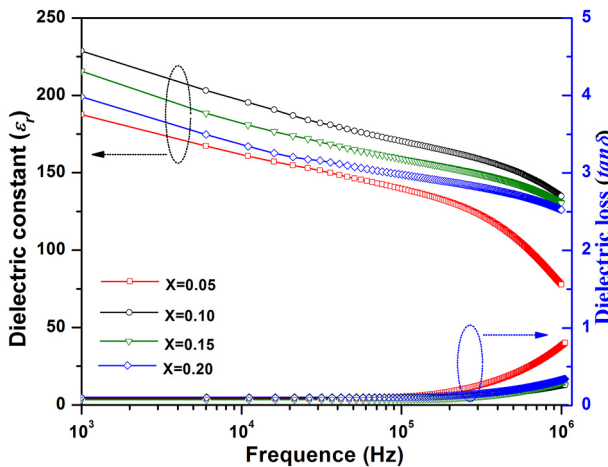


Fig. 6. Variations of  $\epsilon_r$  and  $\tan\delta$  with electric frequency.

phase derived from the excessive Fe and the deterioration of the leakage performance. The impurity phase acted as the defect might segregate at the boundaries, leading to the enhancement of domain wall pinning [67]. In addition, the SCLC conduction mode of the BiTF<sub>0.20</sub>/LSMO film verifies the existence of space charge effect, which also causes pinning effect. The increment domain pinning effect may slow down the motion of domain walls, resulting in the decreased  $P_r$  and increased  $E_c$  [68]. As a whole, the good anti-breakdown characteristic and good leakage performance are beneficial to obtain the better ferroelectric properties [69]. Hence, the BiTF<sub>0.10</sub>/LSMO film with the excellent leakage

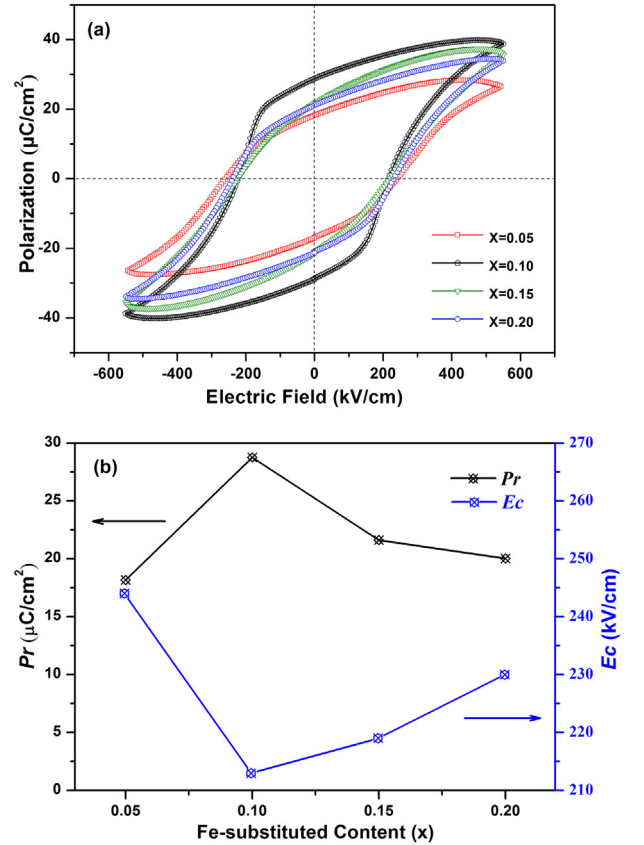


Fig. 7. (a)  $P$ - $E$  hysteresis loops of the BiTF<sub>x</sub>/LSMO films and (b) variation of  $P_r$  and  $E_c$  with Fe-substituted content.

performance exhibits the best ferroelectric properties.

### 3.8. Magnetic properties

To verify that Fe substitution can really make BiTF<sub>0.10</sub> have ferromagnetic properties, BiT film and BiTF<sub>0.10</sub> film were fabricated on the silicon substrate. The preparation process of BiT and BiTF<sub>0.10</sub> films is the same as that of the BiTF<sub>0.10</sub> layer in the BiTF<sub>0.10</sub>/LSMO film. Certainly, no Fe(NO<sub>3</sub>)<sub>3</sub>·9H<sub>2</sub>O is added in the preparation of BiT precursor solution. Fig. 8(a) illustrates the magnetic field ( $H$ ) dependent magnetization ( $M$ ) loop of the BiT film. It can be verified that the pure BiT presents a diamagnetic characterization. The  $M$ - $H$  loop of the BiTF<sub>0.10</sub> film is illustrated in Fig. 8(b). More interestingly, the BiTF<sub>0.10</sub> film demonstrates a soft ferromagnetism characteristic with a saturation magnetization ( $M_s$ ) of 0.65 emu/cm<sup>3</sup>. According to the inset shown in the  $M$ - $H$  loop, it is identified that the coercive field ( $H_c$ ) of BiTF<sub>0.10</sub> film is about 60 Oe. The  $M$ - $H$  loop of the LSMO film deposited on the  $c$ -axis oriented LNO-buffered silicon substrate is shown in Fig. 8(c). Its  $M_s$  and  $H_c$  are 369 emu/cm<sup>3</sup> and 50 Oe (inset (I)), respectively. They can be comparable to the previously reported values by Lu et al. [70]. The  $M$ - $H$  loop of the BiTF<sub>0.10</sub>/LSMO composite film was also examined, and compared with that of the LSMO film. Although BiTF<sub>0.10</sub> phase can contribute to the ferromagnetism of the BiTF<sub>0.10</sub>/LSMO film, the  $M$ - $H$  curve of the BiTF<sub>0.10</sub>/LSMO film is almost coincided with that of the LSMO film. It is due to too weak ferromagnetism of BiTF<sub>0.10</sub> phase, in comparison with that of the LSMO phase. It should be noted from the inset (II) shown in Fig. 8(c) that the  $H_c$  of the BiTF<sub>0.10</sub>/LSMO film is 50 Oe, which is equal to that of the LSMO film.

The magnetism mechanism of the BiTF<sub>0.10</sub> caused by Fe substitution was also investigated by first-principles calculations. The atomic structure model of a perfect BiT is given in Fig. S1(a). In our substitution calculation, a  $\sqrt{2} \times \sqrt{2} \times 1$  supercell containing two BiT formula



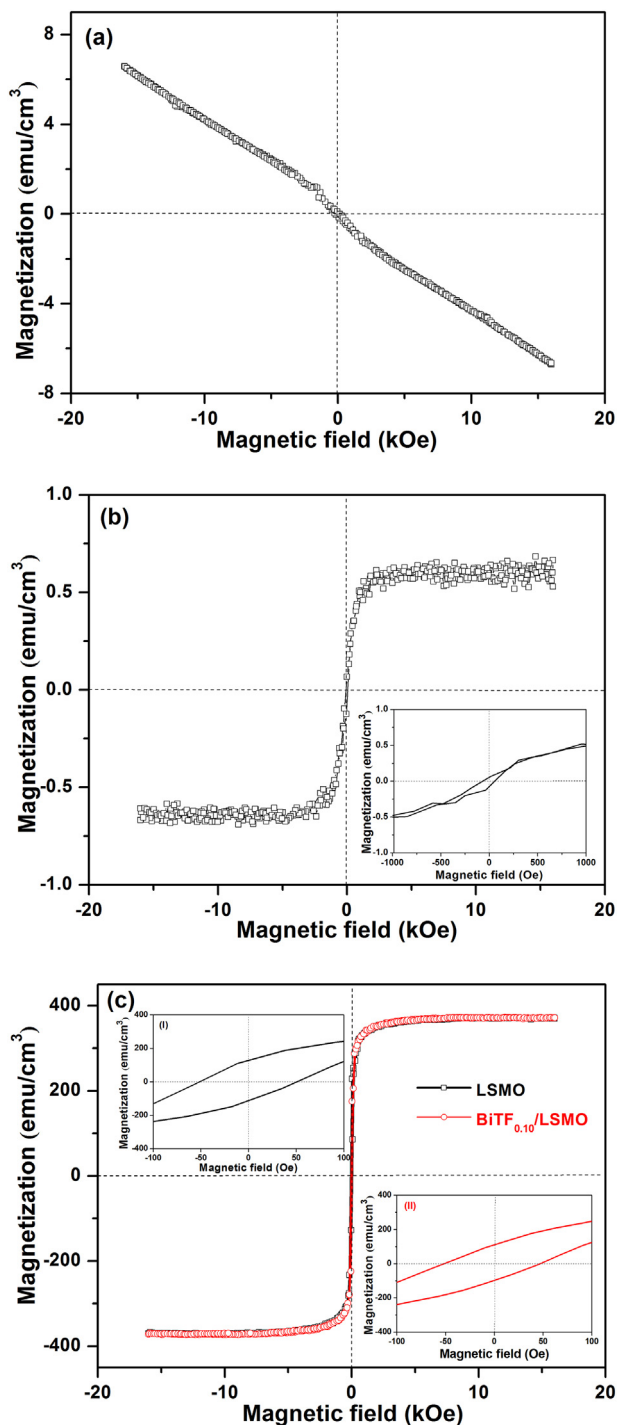


**Fig. 8.** *M-H* loops of (a) BiT, (b) BiTF<sub>0.10</sub>, (c) LSMO and BiTF<sub>0.10</sub>/LSMO films. The inset shown in (b) depicts the partial enlarge view of the *M-H* loop of the BiTF<sub>0.10</sub> film at near zero magnetic field. The insets (I) and (II) of (c) depict the partial enlarge views of the *M-H* loops of LSMO and BiTF<sub>0.10</sub>/LSMO film at near zero magnetic field, respectively.

cells for tetragonal structure was built, and the Fe substitute was introduced by replacing a Ti (B-site), resulting in a substituted concentration of 1/152 (Fig. S1(b)). As shown in Fig. 9(a), the spin density of states for BiTF<sub>0.10</sub> demonstrates that the majority and minority states around the Fermi level are asymmetric, which can induce spin splitting and magnetic moments. Hence, the calculated magnetic moment is  $2\mu_B$  per super cell. To gain more insights of the magnetism, the isosurfaces of the spin density distribution (difference of electronic charge density

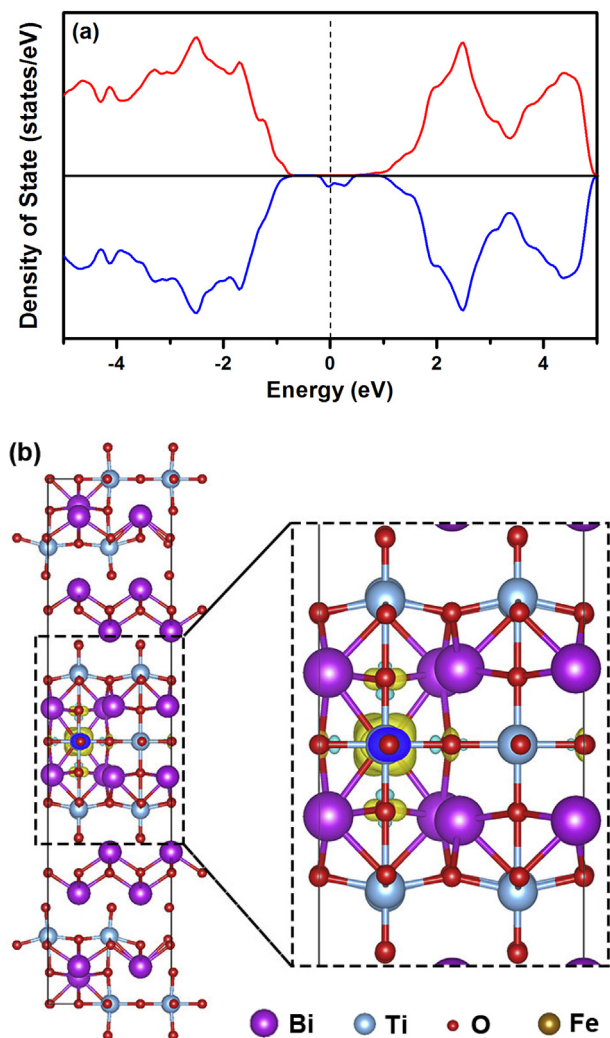


**Fig. 9.** (a) Spin-resolved total density of state for BiTF<sub>0.10</sub>, in which the contribution of the spin-up and spin-down branches were denoted by the red and blue lines, respectively, and the Fermi level was denoted by the dashed line. (b) The isosurfaces of the spin density distribution for BiTF<sub>0.10</sub>.

between spin-up and spin-down channel) were also calculated. As shown in Fig. 9(b), the Fe substitution causes the charge redistribution around Fe ion and neighboring O ions. Therefore, the spin polarized state mainly derives from the 3d orbitals of the Fe ion, and a tiny percent comes from the 2p orbitals of the neighboring O ions, which is also obvious according to the partial density of states of the Fe ion (see Fig. S2).

### 3.9. ME properties

For the magnetoelectric composites, the ME effect is a coupled performance between ferromagnetic and ferroelectric phases via elastic interaction. Thus, the coexistence of excellent ferroelectric and ferromagnetic performances of the BiTF<sub>0.10</sub>/LSMO composite film will benefit to obtain a good ME effect. Its direct ME effect indicated by ME voltage coefficient ( $\alpha_E$ ) can be expressed as:

$$\alpha_E = \frac{\delta E}{\delta H} = \frac{\delta V}{t \times \delta H} = \frac{V_{out}}{(t \times H_{ac})} \quad (3)$$

where  $t$  is the total thickness of the composite film,  $H_{ac}$  the intensity of AC magnetic field and  $V_{out}$  the inductive output voltage. The measurement was carried out at the  $H_{ac}$  of 0.5 Oe under four different frequencies (10, 15, 20 and 25 kHz). Fig. 10 illustrates  $\alpha_E$  as a function of



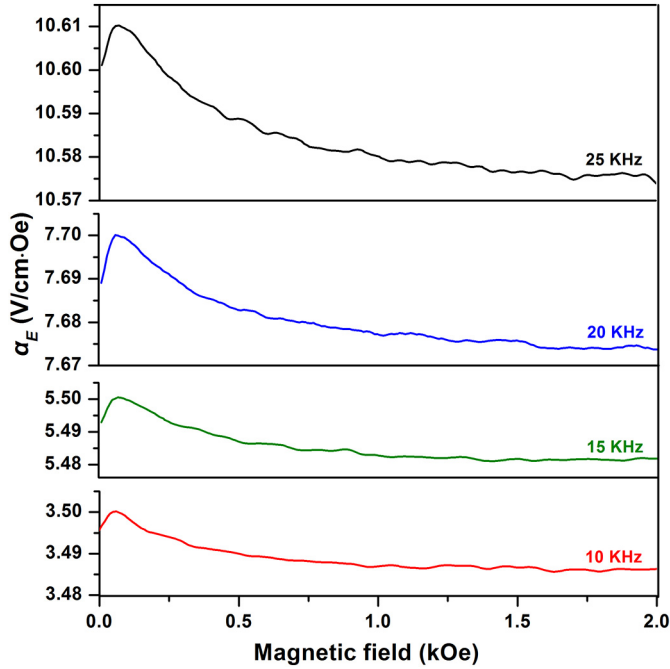


Fig. 10. Variation of  $\alpha_E$  with  $H_{bias}$  of the BiTF<sub>0.10</sub>/LSMO film.

$H_{bias}$ . The  $\alpha_E$  values for all frequencies increase with the applied  $H_{bias}$  till a peak at about  $H_{bias} = 50$  Oe, and then decline progressively. This ME behavior is in agreement with the observation for single-phase multiferroic BiFe<sub>1-x</sub>Mn<sub>x</sub>O<sub>3</sub> ceramics [71], CoFe<sub>2</sub>O<sub>4</sub>-(Ba<sub>0.85</sub>Ca<sub>0.15</sub>)(Zr<sub>0.1</sub>Ti<sub>0.9</sub>)O<sub>3</sub> laminate composites [72], and BaTiO<sub>3</sub>-BiFeO<sub>3</sub> [14] and Ba<sub>0.8</sub>Sr<sub>0.2</sub>Ti<sub>0.9</sub>Zr<sub>0.1</sub>O<sub>3</sub>-Ni<sub>0.8</sub>Zn<sub>0.2</sub>Fe<sub>2</sub>O<sub>4</sub> [73] composite films. The  $H_{bias}$ , 50 Oe, is equal to the  $H_c$  (50 Oe) of the BiTF<sub>0.10</sub>/LSMO composite film. It indicates that the domain wall motion has a larger contribution to ME effect than the domain rotation. The maximum  $\alpha_E$  of the film is 3.5, 5.5, 7.7 and 10.6 V/cm-Oe at 10, 15, 20 and 25 kHz, respectively. To the best of our knowledge, these  $\alpha_E$  values are comparable to many excellent magnetoelectric composite films [11–14]. Moreover, despite of AC frequency, the  $\alpha_E$  of the film is not equal to 0 even if  $H_{bias}$  is 0 Oe. The similar ME behavior was also observed in the films such as Pb(Zr<sub>0.95</sub>Ti<sub>0.05</sub>)O<sub>3</sub>/CoFe<sub>2</sub>O<sub>4</sub> [74] and MnFe<sub>2</sub>O<sub>4</sub>/(Pb,Sr)TiO<sub>3</sub> [75]. It has been reported that this zero-bias ME behavior is likely attributed to the residual field or remnant magnetization [76,77]. Though the plots of  $\alpha_E$  vs.  $H_{bias}$  at different frequencies show the similar tendency, the ME performance is obviously better at high frequency than that at low frequency. Based on this finding, the AC magnetic frequency dependence on  $\alpha_E$  of the film was further studied in the absence of  $H_{bias}$ . As expected, the ME response was very sensitive to the frequency. Fig. 11 shows that the  $\alpha_E$  value increases gradually from 0 with increase of the frequency. Because  $\alpha_E$  has an inverse ratio to  $\epsilon_r$ , the change of  $\epsilon_r$  of the magnetoelectric composite film with frequency is possibly the main reason for the variation of  $\alpha_E$  with AC magnetic frequency [78–80]. As mentioned in Fig. 6, at below 100 kHz,  $\epsilon_r$  decreases with increasing frequency. Consequently, the  $\alpha_E$  of the film increases gradually with increase of the frequency. At 100 kHz (the maximum frequency of the measurement equipment),  $\alpha_E$  can reach up to 47.5 V/cm-Oe. Apparently, it is larger than that of many magnetoelectric composites reported in the literatures [11–14]. There are several possible reasons for the excellent ME performance of the present magnetoelectric composite film. In a layered magnetoelectric composite film, the ME effect mainly derives from the magnetic-mechanical-electric transformations between ferromagnetic and ferroelectric phases through stress-mediated transfers. For the BiTF<sub>0.10</sub>/LSMO film, the BiTF<sub>0.10</sub> phase exhibits good ferroelectric properties. Meanwhile, the LSMO phase has high saturation magnetization and lower  $H_c$ . The lower  $H_c$  suggests an easy-

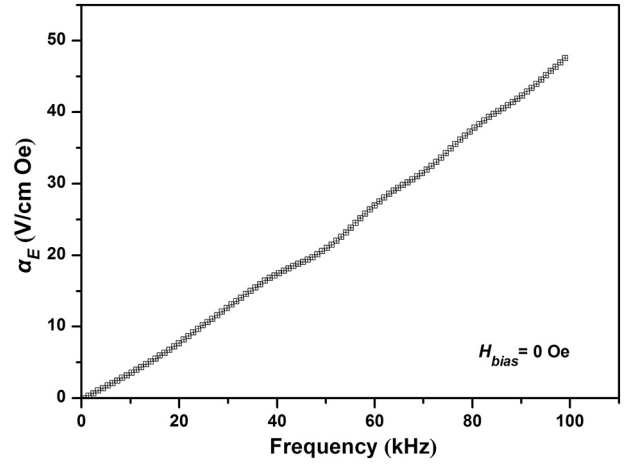


Fig. 11. ME response of the BiTF<sub>0.10</sub>/LSMO film with magnetic frequency in the absence of  $H_{bias}$ .

magnetism characteristic of the LSMO phase, which is advantageous to the motion of magnetic domain walls, resulting in a large magnetostriction even at a low  $H_{bias}$  [81]. Consequently, the interaction between two phases certainly produce an excellent ME performance. Secondly, the BiTF<sub>0.10</sub>/LSMO film exhibits excellent characteristics of oriented growth, large grain size and compact structure, which is beneficial for the stress transfer between ferromagnetic and ferroelectric phases, thus leading to an improved ME effect. Furthermore, as mentioned above, the BiTF<sub>0.10</sub> is a single-phase multiferrous material with good ferroelectricity and weak magnetism. Intrinsic interaction between ferroelectric orders and magnetic orders may causes an additional spontaneous ME effect.

It is well known, that  $H_{bias}$  is essential for the most reported magnetoelectric composites to excite piezomagnetic response to induce ME effect, and usually obtain a larger  $\alpha_E$  value under a  $H_{bias}$  ranging from hundreds to thousands of Oe, but additional requirement of  $H_{bias}$  is problematic for device structure and fabrication [82]. The discovery of magnetoelectric composites with zero-biased ME effect is encouraging, which is beneficial to reduce device volume and eliminate interface effects by additional magnet. The excellent ME response of the BiTF<sub>0.10</sub>/LSMO film in the absence of  $H_{bias}$  suggests its potential use in memorizers, transducers and sensors, etc. Furthermore, the successful integration of the BiTF<sub>0.10</sub>/LSMO film on the silicon substrate can provide an approach for the combination of magnetoelectric composite films with semiconductor materials to fabricate multifunctional devices.

#### 4. Conclusions

In summary, LNO, LSMO and BiTF<sub>x</sub> layers were successively deposited on the silicon substrate using the facile CSD method, and LNO-buffer layer with *c*-axis orientation could act as a seed layer to induce the oriented growth of the overlaying LSMO and BiTF<sub>x</sub> layers. The Fe-substituted content in BiTF<sub>x</sub> phase has a significant effect on the surface morphology, and leakage, dielectric and ferroelectric properties of the corresponding composite films. The optimum Fe-substituted content for BiTF<sub>x</sub> phase is  $x = 0.10$ , and the corresponding composite film exhibits a sole Ohmic conduction mechanism, resulting in an improved leakage performance. The BiTF<sub>0.10</sub>/LSMO film possesses excellent dielectric properties with the largest  $\epsilon_r$  and the least  $\tan\delta$ . In addition, it exhibits the best ferroelectric properties with the highest  $Pr$  of 28.7  $\mu\text{C}/\text{cm}^2$ . More interestingly, BiTF<sub>x</sub> shows weak ferromagnetic properties. The spin density of states for BiTF<sub>0.10</sub> indicates that the majority and minority states are asymmetric around the Fermi level, which can induce spin splitting and magnetic moments. The BiTF<sub>0.10</sub>/LSMO film exhibits

excellent ferroelectric and ferromagnetic properties, resulting in a good ME performance. Furthermore, the ME response is very sensitive to the AC magnetic frequency. The  $\alpha_E$  increases gradually from 0 with increase of the frequency in the absence of  $H_{bias}$ , and the highest  $\alpha_E$  of 47.5 V/cm-Oe can be achieved at 100 kHz.

## Acknowledgement

The authors acknowledge the financial support by the National Natural Science Foundation of China (Nos. 61404107, 51672212, 51801152 and 51771145), Scientific Research Fund of the Education Department of Shaanxi Province (No. 2013JK0676), Natural Science Foundation of Shaanxi Province (No. 2018JM5019) and Opening Project of Material Corrosion and Protection Key Laboratory of Sichuan Province (No. 2015CL07).

## Appendix A. Supplementary data

Supplementary data to this article can be found online at <https://doi.org/10.1016/j.apsusc.2019.06.030>.

## References

- [1] M. Fiebig, Revival of the magnetoelectric effect, *J. Phys. D. Appl. Phys.* 38 (2005) R123–R152.
- [2] W. Eerenstein, N.D. Mathur, J.F. Scott, Multiferroic and magnetoelectric materials, *Nature* 442 (2006) 759–765.
- [3] N.A. Spaldin, M. Fiebig, The renaissance of magnetoelectric multiferroics, *Science* 309 (2005) 391–392.
- [4] C.-W. Nan, M.I. Bichurin, S. Dong, D. Viehland, G. Srinivasan, Multiferroic magnetoelectric composites: historical perspective, status, and future directions, *J. Appl. Phys.* 103 (2008) 031101.
- [5] S.R. Spurgeon, P.V. Balachandran, D.M. Kepaptsoglou, A.R. Damodaran, J. Karthik, S. Nejat, L. Jones, H. Ambaye, V. Lauter, Q.M. Ramasse, K.K.S. Lau, L.W. Martin, J.M. Rondinelli, M.L. Taheri, Polarization screening-induced magnetic phase gradients at complex oxide interfaces, *Nat. Commun.* 6 (2015) 6735.
- [6] G. Lawes, G. Srinivasan, Introduction to magnetoelectric coupling and multiferroic films, *J. Phys. D. Appl. Phys.* 44 (2011) 243001.
- [7] M. Bibes, A. Barthélemy, Towards a magnetoelectric memory, *Nat. Mater.* 7 (2008) 425–426.
- [8] A.P. Pyatakov, A.K. Zvezdin, Magnetoelectric and multiferroic media, *Phys-Usp* + 55 (2012) 557–581.
- [9] N. Castro, S. Reis, M.P. Silva, V. Correia, S. Lanceros-Mendez, P. Martins, Development of a contactless DC current sensor with high linearity and sensitivity based on the magnetoelectric effect, *Smart Mater. Struct.* 27 (2018) 065012.
- [10] Z. Chu, M. PourhosseiniAsl, S. Dong, Review of multi-layered magnetoelectric composite materials and devices applications, *J. Phys. D. Appl. Phys.* 51 (2018) 243001.
- [11] Y. Shi, Y. Gao, A quasistatic hysteresis model for magnetoelectric effect in multiferroic nanostructured films with surface effect, *J. Alloys Compd.* 762 (2018) 706–718.
- [12] H. Modarresi, V. Lazenka, E. Menéndez, M. Lorenz, M. Bisht, A. Volodin, C. Van Haesendonck, M. Grundmann, M.J. Van Bael, K. Temst, A. Vantomme, Induced ferromagnetism and magnetoelectric coupling in ion-beam synthesized BiFeO<sub>3</sub>-CoFe<sub>2</sub>O<sub>4</sub> nanocomposite thin films, *J. Phys. D. Appl. Phys.* 49 (2016) 325302.
- [13] P.P. Ortega, L.S.R. Rocha, C.C. Silva, M. Cilense, R.A.C. Amoresi, E. Longo, A.Z. Simões, Multiferroic behavior of heterostructures composed of lanthanum and bismuth ferrite, *Ceram. Int.* 42 (2016) 16521–16528.
- [14] M. Lorenz, V. Lazenka, P. Schwinkendorf, F. Bern, M. Ziese, H. Modarresi, A. Volodin, M.J. Van Bael, K. Temst, A. Vantomme, M. Grundmann, Multiferroic BaTiO<sub>3</sub>-BiFeO<sub>3</sub> composite thin films and multilayers: strain engineering and magnetoelectric coupling, *J. Phys. D. Appl. Phys.* 47 (2014) 135303.
- [15] X.L. Zhong, M. Liao, J.B. Wang, S.H. Xie, Y.C. Zhou, Structural, ferroelectric, ferromagnetic, and magnetoelectric properties of the lead-free Bi<sub>3.15</sub>Nd<sub>0.85</sub>Ti<sub>3</sub>O<sub>12</sub>/CoFe<sub>2</sub>O<sub>4</sub> double-layered thin film, *J. Cryst. Growth* 310 (2008) 2995–2998.
- [16] H.N. Lee, D. Hesse, N. Zakharov, U. Gösele, Ferroelectric Bi<sub>3.25</sub>La<sub>0.75</sub>Ti<sub>3</sub>O<sub>12</sub> films of uniform a-axis orientation on silicon substrates, *Science* 296 (2002) 2006–2009.
- [17] Z. Duan, Y. Cui, G. Zhao, X. Li, B. Peng, C. Han, Integration of c-axis oriented Bi<sub>3.15</sub>Nd<sub>0.85</sub>Ti<sub>2.95</sub>Hf<sub>0.05</sub>O<sub>12</sub>/La<sub>0.67</sub>Sr<sub>0.33</sub>MnO<sub>3</sub> ferromagnetic-ferroelectric composite film on Si substrate, *Sci. Rep.* 7 (2017) 11341.
- [18] A. Rani, J. Kolte, P. Gopalan, Structural, electrical, magnetic and magnetoelectric properties of Co-doped BaTiO<sub>3</sub> multiferroic ceramics, *Ceram. Int.* 44 (2018) 16703–16711.
- [19] G. Gong, Y. Fang, G. Zerihun, C. Yin, S. Huang, S. Yuan, Investigation of A-site La substituted BaTi<sub>0.96</sub>Mn<sub>0.04</sub>O<sub>3</sub> ceramics: searching for ferromagnetic origin, *J. Appl. Phys.* 115 (2014) 243902.
- [20] Y.-H. Lin, J. Yuan, S. Zhang, Y. Zhang, J. Liu, Y. Wang, C.-W. Nan, Multiferroic behavior observed in highly orientated Mn-doped BaTiO<sub>3</sub> thin films, *Appl. Phys. Lett.* 95 (2009) 033105.
- [21] M. Kumar, K.L. Yadav, Study of dielectric, magnetic, ferroelectric and magnetoelectric properties in the PbMn<sub>1-x</sub>O<sub>3</sub> system at room temperature, *J. Phys. Condens. Matter* 19 (2007) 242202.
- [22] F. Craciun, E. Dimitriu, M. Grigoras, N. Lupu, Multiferroic perovskite (Pb<sub>0.845</sub>Sm<sub>0.08</sub>Fe<sub>0.035</sub>)(Ti<sub>0.98</sub>Mn<sub>0.02</sub>)O<sub>3</sub> with ferroelectric and weak ferromagnetic properties, *Appl. Phys. Lett.* 102 (2013) 242903.
- [23] H. Zhao, H. Kimura, Z. Cheng, M. Osada, J. Wang, X. Wang, S. Dou, Y. Liu, J. Yu, T. Matsumoto, T. Tohei, N. Shibata, Y. Ikuhara, Large magnetoelectric coupling in magnetically short-range ordered Bi<sub>5</sub>Ti<sub>3</sub>FeO<sub>15</sub> film, *Sci. Rep.* 4 (2014) 5255.
- [24] J.Y. Han, C.W. Bark, Structural and optical properties of Fe doped bismuth titanate thin film deposited by RF sputtering, *Jpn. J. Appl. Phys.* 55 (2016) 02BC09.
- [25] J. Paul, S. Bhardwaj, K.K. Sharma, R.K. Kotnala, R. Kumar, Room temperature multiferroic behaviour and magnetoelectric coupling in Sm/Fe modified Bi<sub>4</sub>Ti<sub>3</sub>O<sub>12</sub> ceramics synthesized by solid state reaction method, *J. Alloys Compd.* 634 (2015) 58–64.
- [26] R. Ti, X. Lu, J. He, F. Huang, H. Wu, F. Mei, M. Zhou, Y. Li, T. Xu, J. Zhu, Multiferroic properties and magnetoelectric coupling in Fe/Co co-doped Bi<sub>3.25</sub>La<sub>0.75</sub>Ti<sub>3</sub>O<sub>12</sub> ceramics, *J. Mater. Chem. C* 3 (2015) 11868–11873.
- [27] R. Tang, J.Y. Han, J.H. Kim, C.W. Bark, Optimal doping level of iron in bismuth titanate for oxide optoelectronics, *J. Nanosci. Nanotechnol.* 17 (2017) 7307–7311.
- [28] M.S. Shashkov, O.V. Malyshkina, I.V. Piir, M.S. Koroleva, Dielectric properties of iron-containing bismuth titanate solid solutions with a layered perovskite structure, *Phys. Solid State* 57 (2015) 518–521.
- [29] X.Q. Chen, F.J. Yang, W.Q. Cao, H. Wang, C.P. Yang, D.Y. Wang, K. Chen, Enhanced multiferroic characteristics in Fe-doped Bi<sub>4</sub>Ti<sub>3</sub>O<sub>12</sub> ceramics, *Solid State Commun.* 150 (2010) 1221–1224.
- [30] A. Xia, G. Tan, H. Ren, Effect of Fe substitution on microstructure and properties of bismuth titanate thin films, *Ceram. Int.* 42 (2016) 1267–1271.
- [31] M.-S. Chen, T.-B. Wu, J.-M. Wu, Effect of textured LaNiO<sub>3</sub> electrode on the fatigue improvement of Pb(Zr<sub>0.53</sub>Ti<sub>0.47</sub>)O<sub>3</sub> thin films, *Appl. Phys. Lett.* 68 (1996) 1430–1432.
- [32] H. Suzuki, Y. Miwa, T. Naoe, H. Miyazaki, T. Ota, M. Fuji, M. Takahashi, Orientation control and electrical properties of PZT/LNO capacitor through chemical solution deposition, *J. Eur. Ceram. Soc.* 26 (2006) 1953–1956.
- [33] W.L. Li, T.D. Zhang, D. Xu, Y.F. Hou, W.P. Cao, W.D. Fei, LaNiO<sub>3</sub> seed layer induced enhancement of piezoelectric properties in (100)-oriented (1-x)BZT-xBCT thin films, *J. Eur. Ceram. Soc.* 35 (2015) 2041–2049.
- [34] A.Z. Simões, E.C. Aguiar, C.S. Riccardi, E. Longo, J.A. Varela, Fatigue and retention properties of Bi<sub>3.25</sub>La<sub>0.75</sub>Ti<sub>3</sub>O<sub>12</sub> films using LaNiO<sub>3</sub> bottom electrodes, *Mater. Charact.* 60 (2009) 353–356.
- [35] G. Srinivasan, E.T. Rasmussen, B.J. Levin, R. Hayes, Magnetoelectric effects in bilayers and multilayers of magnetostrictive and piezoelectric perovskite oxides, *Phys. Rev. B* 65 (2002) 134402.
- [36] Z. Duan, Y. Cui, Z. Yang, K. Li, Y. Wan, Z. Lu, Y. Xie, J. Zhang, Growth of highly c-axis oriented LaNiO<sub>3</sub> films with improved surface morphology on Si substrate using chemical solution deposition and rapid heat treatment process, *Ceram. Int.* 44 (2018) 695–702.
- [37] Z. Duan, X. Shi, Y. Cui, Y. Wan, Z. Lu, G. Zhao, Ferromagnetic, ferroelectric and magnetoelectric properties of (001)-oriented Pb(Zr<sub>0.52</sub>Ti<sub>0.48</sub>)O<sub>3</sub>/La<sub>0.67</sub>Sr<sub>0.33</sub>MnO<sub>3</sub> composite films deposited on Si substrates using chemical solution deposition, *J. Alloys Compd.* 698 (2017) 276–283.
- [38] G. Kresse, J. Hafner, Ab initio molecular dynamics for liquid metals, *Phys. Rev. B* 47 (1993) 558–561.
- [39] P.E. Blöchl, Projector augmented-wave method, *Phys. Rev. B* 50 (1994) 17953–17979.
- [40] J.P. Perdew, K. Burke, M. Ernzerhof, Generalized gradient approximation made simple, *Phys. Rev. Lett.* 77 (1996) 3865–3868.
- [41] H.J. Monkhorst, J.D. Pack, Special points for Brillouin-zone integrations, *Phys. Rev. B* 13 (1976) 5188–5192.
- [42] K. Nishimura, T. Yoshioka, T. Yamamoto, Substitution mechanism of Mn and Fe ions in Bi<sub>4</sub>Ti<sub>3</sub>O<sub>12</sub>, *IEEE Trans. Magn.* 50 (2014) 2502306.
- [43] J. Wu, J. Wang, BiFeO<sub>3</sub> thin films deposited on LaNiO<sub>3</sub>-buffered SiO<sub>2</sub>/Si substrate, *J. Am. Ceram. Soc.* 93 (2010) 1422–1426.
- [44] C.M. Raghavan, J.W. Kim, J.Y. Choi, J.-W. Kim, S.S. Kim, Effects of donor W<sup>6+</sup>-ion doping on the microstructural and multiferroic properties of Aurivillius Bi<sub>7</sub>Fe<sub>3</sub>Ti<sub>3</sub>O<sub>21</sub> thin film, *Appl. Surf. Sci.* 346 (2015) 201–206.
- [45] W.L. Liu, H.R. Xia, H. Han, X.Q. Wang, Structural, morphology and electrical studies of Sm-modified bismuth titanate thin films on Si (100), *J. Solid State Chem.* 177 (2004) 3021–3027.
- [46] X. Chen, J. Xiao, Y. Xue, X. Zeng, F. Yang, P. Su, Room temperature multiferroic properties of Ni-doped Aurivillius phase Bi<sub>5</sub>Ti<sub>3</sub>FeO<sub>15</sub>, *Ceram. Int.* 40 (2014) 2635–2639.
- [47] R.D. Shannon, Revised effective ionic radii and systematic studies of interatomic distances in halides and chalcogenides, *Acta Cryst. A* 32 (1976) 751–767.
- [48] J. Liang, G. Zhu, P. Liu, X. Luo, C. Tan, L. Jin, J. Zhou, Synthesis and characterization of Fe-doped  $\beta$ -Bi<sub>2</sub>O<sub>3</sub> porous microspheres with enhanced visible light photocatalytic activity, *Superlattice. Microsc.* 72 (2014) 272–282.
- [49] Z. Duan, Y. Zhu, P. Ren, J. Jia, S. Yang, G. Zhao, Y. Xie, J. Zhang, Non-UV activated superhydrophilicity of patterned Fe-doped TiO<sub>2</sub> film for anti-fogging and photocatalysis, *Appl. Surf. Sci.* 452 (2018) 165–173.
- [50] S. Wang, J.S. Lian, W.T. Zheng, Q. Jiang, Photocatalytic property of Fe doped anatase and rutile TiO<sub>2</sub> nanocrystal particles prepared by sol-gel technique, *Appl. Surf. Sci.* 263 (2012) 260–265.
- [51] J.H. Kim, Y.J. Jang, J.H. Kim, J.-W. Jang, S.H. Choi, J.S. Lee, Defective ZnFe<sub>2</sub>O<sub>4</sub> nanorods with oxygen vacancy for photoelectrochemical water splitting, *Nanoscale* 7 (2015) 19144–19151.

- [52] X. Zhu, S. Li, X. Yang, J. Qiu, Microstructures and electrical properties of  $\text{La}_{0.8}\text{Sr}_{0.2}\text{MnO}_3$  films synthesized by sol-gel method, *Appl. Surf. Sci.* 254 (2007) 532–537.
- [53] S.-Y. Lee, B.-O. Park, Microstructure and ferroelectric properties of Nb-doped  $\text{Bi}_4\text{Ti}_3\text{O}_{12}$  thin films prepared by sol-gel method, *J. Cryst. Growth* 283 (2005) 81–86.
- [54] J.K. Kim, T.K. Song, S.S. Kim, J. Kim, Ferroelectric properties of tungsten-doped bismuth titanate thin film prepared by sol-gel route, *Mater. Lett.* 57 (2002) 964–968.
- [55] C.M. Raghavan, J.W. Kim, J.Y. Choi, J.-W. Kim, S.S. Kim, Investigation of structural, electrical and multiferroic properties of Co-doped Aurivillius  $\text{Bi}_6\text{Fe}_2\text{Ti}_3\text{O}_{18}$  thin films, *Ceram. Int.* 41 (2015) 3277–3282.
- [56] F.-C. Chiu, A review on conduction mechanism in dielectric films, *Adv. Mater. Sci. Eng.* 2014 (2014) 1–18.
- [57] C.H. Yang, S.D. Wang, D.M. Yang, Fabrication and properties of silicon-based  $(\text{Bi},\text{Sm})_4\text{Ti}_3\text{O}_{12}$  thin film, *J. Alloys Compd.* 467 (2009) 434–437.
- [58] P.C. Joshi, S.B. Desu, Structural and electrical characteristics of rapid thermally processed ferroelectric  $\text{Bi}_4\text{Ti}_3\text{O}_{12}$  thin films prepared by metalorganic solution deposition technique, *J. Appl. Phys.* 80 (1996) 2349–2357.
- [59] J. Kim, J.K. Kim, S. Heo, H.S. Lee, Ferroelectric properties of sol-gel prepared La- and Nd-substituted, and Nb-co-substituted bismuth titanate using polymeric additives, *Thin Solid Films* 503 (2006) 60–63.
- [60] T. Watanabe, H. Funakubo, M. Osada, Y. Noguchi, M. Miyayama, Effect of cosubstitution of La and V in  $\text{Bi}_4\text{Ti}_3\text{O}_{12}$  thin films on the low-temperature deposition, *Appl. Phys. Lett.* 80 (2002) 100–102.
- [61] L. Wang, C. Chen, Z. Tang, C. Lu, B. Yu, Dependence of Zr content on electrical properties of  $\text{Bi}_{3.15}\text{Nd}_{0.85}\text{Ti}_{3-x}\text{Zr}_x\text{O}_{12}$  thin films synthesized by chemical solution deposition (CSD), *Vacuum* 85 (2010) 203–206.
- [62] X. Hu, A. Garg, Z.H. Barber, Structural and electrical properties of samarium-substituted bismuth titanate ferroelectric thin films on  $\text{Pt}/\text{TiO}_2/\text{SiO}_2/\text{Si}$  substrates, *Thin Solid Films* 484 (2005) 188–195.
- [63] M.-C. Kao, H.-Z. Chen, S.-L. Young, The microstructure and ferroelectric properties of Sm and Ta-doped bismuth titanate ferroelectric thin films, *Thin Solid Films* 528 (2013) 143–146.
- [64] L. Yan, L.B. Kong, C.K. Ong, Pulsed laser deposition and characterization of  $\text{Bi}_{3.25}\text{Nd}_{0.75}\text{Ti}_3\text{O}_{12}$  thin films buffered with  $\text{La}_{0.7}\text{Sr}_{0.3}\text{MnO}_3$  electrode, *Mater. Lett.* 58 (2004) (2953–2597).
- [65] X.P. Wang, J. Zhu, W.B. Luo, Y. Zhang, Y.R. Li, Enhanced ferroelectric properties of Hf-doped bismuth titanate thin films on STO (111) substrates, *J. Appl. Phys.* 104 (2008) 074112.
- [66] Y. Chen, Z. Pen, Q. Wang, J. Zhu, Crystalline structure, ferroelectric properties, and electrical conduction characteristics of W/Cr co-doped  $\text{Bi}_4\text{Ti}_3\text{O}_{12}$  ceramics, *J. Alloys Compd.* 612 (2014) 120–125.
- [67] X. Du, W. Huang, S. He, T. Santhosh Kumar, A. Hao, N. Qin, D. Bao, Dielectric, ferroelectric, and photoluminescent properties of Sm-doped  $\text{Bi}_4\text{Ti}_3\text{O}_{12}$  thin films synthesized by sol-gel method, *Ceram. Int.* 44 (2018) 19402–19407.
- [68] P. Gautam, S.K. Singh, R.P. Tandon, Mechanism for leakage current conduction in manganese doped  $\text{Bi}_{3.25}\text{La}_{0.75}\text{Ti}_3\text{O}_{12}$  (BLT) ferroelectric thin films, *J. Alloys Compd.* 606 (2014) 132–138.
- [69] Y. Noguchi, M. Miyayama, Large remanent polarization of vanadium-doped  $\text{Bi}_4\text{Ti}_3\text{O}_{12}$ , *Appl. Phys. Lett.* 78 (2001) 1903–1905.
- [70] Y. Lu, X.W. Li, G.Q. Gong, G. Xiao, A. Gupta, P. Lecoeur, J.Z. Sun, Y.Y. Wang, V.P. Dravid, Large magnetotunneling effect at low magnetic fields in micrometer-scale epitaxial  $\text{La}_{0.67}\text{Sr}_{0.33}\text{MnO}_3$  tunnel junctions, *Phys. Rev. B* 54 (1996) R8357–R8360.
- [71] Y. Li, S.D. Zhou, L. Zhu, Y.G. Wang, Structural transition and its effect on magnetoelectric coupling in the  $\text{BiFe}_{1-x}\text{Mn}_x\text{O}_3$  ceramics prepared by sol-gel method, *J. Magn. Magn. Mater.* 465 (2018) 784–788.
- [72] J.P. Praveen, V.R. Monaji, E. Chandrakala, S. Indla, S.D. kumar, V. Subramanian, D. Das, Enhanced magnetoelectric coupling in Ti and Ce substituted lead free CFO-BCZT laminate composites, *J. Alloys Compd.* 750 (2014) 392–400.
- [73] M. Shi, X. Zhang, R. Zuo, Y. Xu, L. Wang, L. Xie, G. Qiu, Multiferroic and magnetoelectric properties of lead-free  $\text{Ba}_{0.8}\text{Sr}_{0.2}\text{Ti}_{0.9}\text{Zr}_{0.1}\text{O}_3\text{-Ni}_{0.8}\text{Zn}_{0.2}\text{Fe}_2\text{O}_4$  composite films with different deposition sequence, *Ceram. Int.* 44 (2018) 16624–16631.
- [74] K. Tahmasebi, A. Barzegar, J. Ding, T.S. Heng, A. Huang, S. Shannigrahi, Magnetoelectric effect in  $\text{Pb}(\text{Zr}_{0.95}\text{Ti}_{0.05})\text{O}_3$  and  $\text{CoFe}_2\text{O}_4$  heteroepitaxial thin film composite, *Mater. Design* 32 (2011) 2370–2373.
- [75] K. Bala, R.K. Kotnala, N.S. Negi, Magnetically tunable dielectric, impedance and magnetoelectric response in  $\text{MnFe}_2\text{O}_4/(\text{Pb}_{1-x}\text{Sr}_x)\text{TiO}_3$  composites thin films, *J. Magn. Magn. Mater.* 424 (2017) 256–266.
- [76] R. Ade, T. Karthik, J. Kolte, V. Sambasiva, A.R. Kulkarni, N. Venkataramani, Room temperature magnetoelectric and magnetodielectric properties of 2-2 bilayer  $0.50\text{Pb}(\text{Ni}_{1/3}\text{Nb}_{2/3})\text{O}_3\text{-}0.35\text{PbTiO}_3\text{-}0.15\text{PbZrO}_3/\text{CoFe}_2\text{O}_4$  thin film, *Scr. Mater.* 150 (2018) 125–129.
- [77] Y. Zhou, S.C. Yang, D.J. Apo, D. Maurya, S. Priya, Tunable self-biased magnetoelectric response in homogenous laminates, *Appl. Phys. Lett.* 101 (2012) 232905.
- [78] G. Srinivasan, E.T. Rasmussen, J. Gallegos, R. Srinivasan, Magnetoelectric bilayer and multilayer structures of magnetostrictive and piezoelectric oxides, *Phys. Rev. B* 64 (2001) 214408.
- [79] T. Li, H. Wang, K. Li, Z. Hu, D. Ma, Correlation between magnetoelectric coupling effect and dielectric properties of  $\text{La}_{0.7}\text{Sr}_{0.3}\text{MnO}_3/\text{BaTiO}_3$  bilayer heterostructure, *Mater. Res. Bull.* 94 (2017) 160–163.
- [80] Q.H. Jiang, Z.J. Shen, J.P. Zhou, Z. Shi, C.-W. Nan, Magnetoelectric composites of nickel ferrite and lead zirconate titanate prepared by spark plasma sintering, *J. Eur. Ceram. Soc.* 27 (2007) 279–284.
- [81] J.G. Wan, X.W. Wang, Y.J. Wu, M. Zeng, Y. Wang, H. Jiang, W.Q. Zhou, G.H. Wang, J.-M. Liu, Magnetoelectric  $\text{CoFe}_2\text{O}_4\text{-Pb}(\text{Zr},\text{Ti})\text{O}_3$  composite thin films derived by a sol-gel process, *Appl. Phys. Lett.* 86 (2005) 122501.
- [82] S.C. Yang, K.-H. Cho, C.-S. Park, S. Priya, Self-biased converse magnetoelectric effect, *Appl. Phys. Lett.* 99 (2011) 202904.